Article

Tropospheric GOM at the Pic du Midi Observatory – correcting bias in denuder based observations

Nicolas Marusczak, Jeroen E. Sonke, Xuewu Fu, and Martin Jiskra

Environ. Sci. Technol., **Just Accepted Manuscript** • Publication Date (Web): 14 Dec 2016

Tropospheric GOM at the Pic du Midi Observatory – correcting bias in denuder based observations

Nicolas Marusczak[†], Jeroen E. Sonke[†,*], Xuewu Fu[†,¥], and Martin Jiskra[†]

[†]Observatoire Midi-Pyrénées, Laboratoire Géosciences Environnement Toulouse, CNRS/IRD/Université de Toulouse, 14, avenue Édouard Belin, 31400 Toulouse, France

[¥]Present address: State Key Laboratory of Environmental Geochemistry, Institute of Geochemistry, Chinese Academy of Sciences, Guiyang, China.

*Corresponding Author: Tel. +33 561332606, Fax: +33 561332560, Email : sonke@get.obs-mip.fr

Abstract

Gaseous elemental mercury (GEM, Hg) emissions are transformed to divalent reactive Hg (RM) forms throughout the troposphere and stratosphere. RM is often operationally quantified as the sum of particle bound Hg (PBM) and gaseous oxidized Hg (GOM). The measurement of GOM and PBM is challenging and under mounting criticism. Here we intercompare six months of automated GOM and PBM measurements using a Tekran® (TK) KCl-coated denuder and quartz regenerable particulate filter method (GOM_{TK}, PBM_{TK}, and RM_{TK}) with RM_{CEM} collected on cation exchange membranes (CEMs) at the high altitude Pic du Midi Observatory. We find that RM_{TK} is systematically lower by a factor of 1.3 than RM_{CEM}. We observe a significant relationship between GOM_{TK} (but not PBM_{TK}) and Tekran® $flush_{TK}$ blanks suggesting significant loss (32%) of labile GOM_{TK} from the denuder or inlet. Adding the $flush_{TK}$ blank to RM_{TK} results in good agreement with RM_{CEM} (slope=1.01, r^2=0.90) suggesting we can correct bias in RM_{TK} and GOM_{TK}. We provide a bias corrected (*) Pic du Midi dataset for 2012-2014 that shows GOM* and RM* levels in dry free tropospheric air of 198±57 and 229±58 pg m^{-3} which agree well with in-flight observed RM and with model based GOM and RM estimates.

TOC Art:

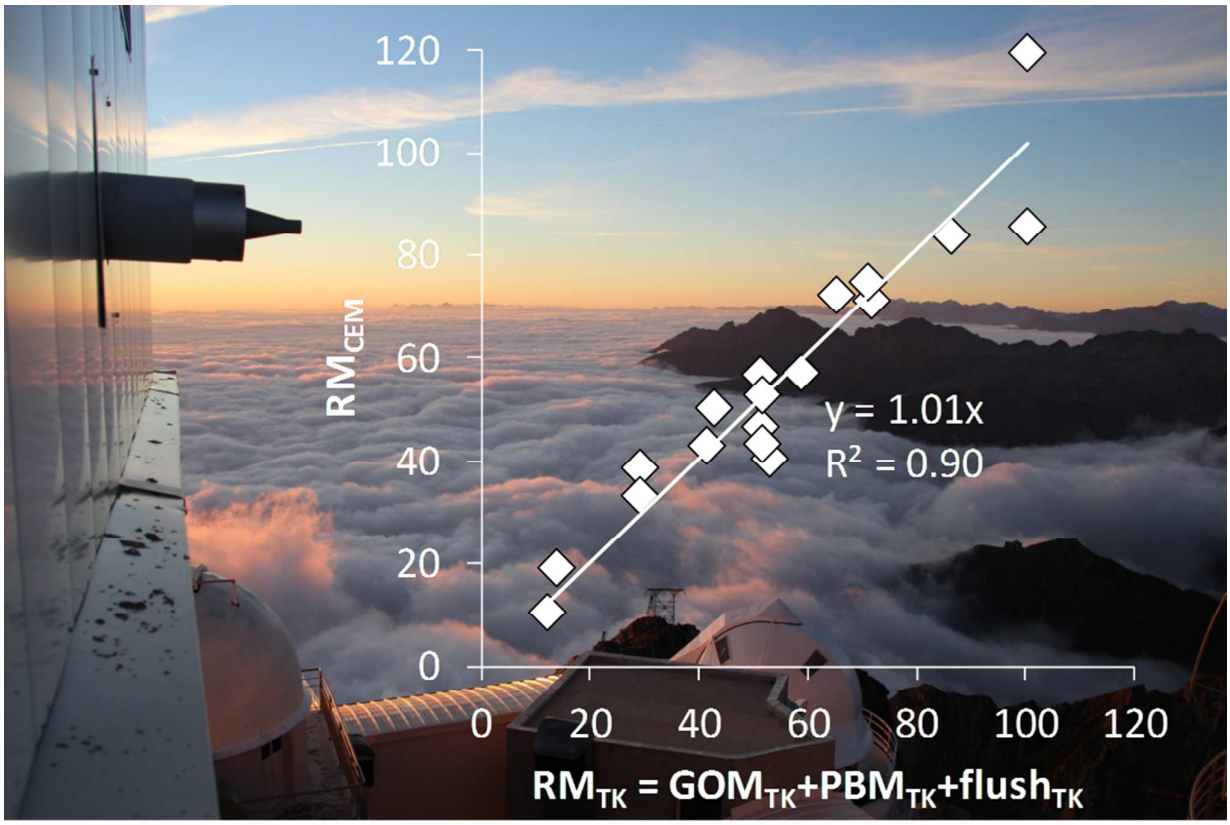

Image credit: Jeroen Sonke

1. Introduction:

Mercury (Hg) is a pollutant of global concern with anthropogenic emissions outweighing natural volcanic emissions by an order of magnitude [1]. Due to its long atmospheric lifetime, on the order of 4 to 12 months, atmospheric circulation carries gaseous elemental Hg (GEM) emissions across the globe and into the upper troposphere and stratosphere [2-4]. Apart from wet deposition, four operationally defined forms of atmospheric Hg have been studied and/or monitored: GEM, gaseous oxidized mercury (GOM), particulate bound mercury (PBM), or divalent reactive Hg (RM), which is the sum of GOM and PBM. In the lower troposphere GOM and PBM are rapidly (days-weeks) transferred to the Earth's surface via wet (*i.e*. rain and snow fall) and dry deposition (Lindberg *et al*., 2007). In the upper troposphere and stratosphere, GOM and PBM have longer lifetimes on the order of weeks to months [5]. GEM emissions can be transformed to RM by oxidation, but the exact nature of the oxidant(s) (O_3, OH and Br, NO_x) and the produced oxidized forms of Hg ($HgCl_2$, $HgBr_2$, HgO, $HgNO_3$, $HgSO_4$, PBM) are topics of debate [6-10].

Operational quantification of GOM, PBM, or RM has been performed by a variety of techniques including sequential oxidizing solution traps (Ontario-Hydro method)[11], mist chambers [12], KCl-coated tubular and annular denuders [13, 14], cation exchange membranes [15-17], indirect difference-based RM (as total mercury (TM) – GEM[18-20]), and chemical ionization mass spectrometry [21]. KCl-coated denuders and regenerable quartz filters have been integrated in automated atmospheric Hg speciation analyzers [13]. The automated speciation systems have permitted great advances in our understanding of atmospheric Hg dynamics, and have become the workhorse of modern Hg speciation monitoring networks such as AMNet, GMOS and CAMnet [22-24].

Previous research has identified analytical issues with KCl-coated denuder based GOM sampling. Interferences with relative humidity and ambient levels of ozone affect GOM adsorption to KCl [25-28]. The RAMIX project extensively investigated different GOM detection methods [29, 30]. It was observed that cation exchange membranes (CEM) collect between 1.3 and 3.7 times more Hg than KCl-denuders in laboratory and field experiments [16, 26]. Criticism on GOM (and PBM) sampling with denuders is mounting and emphasizes the need for better calibration and identification methods for GOM and renewed

development of alternative methods [31]. The observed inefficiencies of GOM collection by KCl-coated denuders illustrate the operational and qualitative nature of the method. Given the wealth of observations made with automated denuder based Hg speciation systems over the past decade it is also of interest to develop a GOM and/or RM loss correction method and, where possible, re-evaluate datasets acquired over the past 15 years.

In this study we compare manual CEM sampling of RM to automated KCl-denuder and quartz filter sampling of GOM and PBM using a Tekran® 1130/1135/2537B system at the high altitude Pic du Midi Observatory (2877m asl, French Pyrenees). In addition, we discuss remarkable, but recurring, observations on denuder flush blanks in relation to GOM levels. The ensemble of automated and manual RM observations allows us to propose a RM and GOM loss correction method for the Pic du Midi dataset.

2. Methods:

2.1. Sampling Site

The Pic du Midi Observatory (PDM, 42.937 N, 0.142 E, 2877 m a.s.l) is a high-altitude site situated on the northern edge of the Pyrenees mountains (France). PDM typically receives free tropospheric air masses from the North Atlantic Ocean and continental Europe. PDM has no nearby anthropogenic emission point sources, but does receive polluted boundary layer air masses from nearby valleys during daytime upslope winds [32, 33].

2.2. Automated Hg speciation measurements

From 18th November 2011 to 31th December 2014, GEM_{TK}, GOM_{TK} and PBM_{TK} were continuously measured at The Pic du Midi observatory, using a Hg speciation unit (1130/1135) coupled to a 2537B analyser (Tekran Inc., Canada). All Tekran® 2537B/1130/1135 components are housed in-doors at PDM due to high lightning risk in summer and abundant ice riming the rest of the year. Ambient air was provided to the Tekran® unit using the Tekran® 1104 Teflon coated, heated (50^{o}C) manifold, operating at 100 L min^{-1}. GOM_{TK}, PBM_{TK} and GEM_{TK} are sampled through KCl-coated denuder, quartz fiber filter and dual gold cartridges respectively.

GEM_{TK} was collected every 5 minutes at 0.7 L min^{-1} and GOM_{TK} and PBM_{TK} are collected at one hour intervals at a flow rate of 5.6 L min^{-1} (flow rates relative to standard conditions, i.e. 273.14^{o}K and 1013 hPa). Detailed standard operating procedures (SOPs), based on Tekran® manuals and consistent with AMNet and GMOS SOPs, QA/QC and results for the period 18/11/2011 to 17/11/2012 have been presented elsewhere [33]. In this study GOM_{TK} and PBM_{TK} are calculated without subtraction of the flush blank in order to evaluate the behaviour of the flush blank itself. The full 2012-2014 PDM dataset is provided in the supporting information (SI-1). A calibration error for the year 2012 was corrected leading to lower GEM values than in [REF] (1.54 instead of 1.86 ng m^{-3}), and consistent annual mean GEM values for 2012, 2013, 2014 of 1.54, 1.54, and 1.53 ng m^{-3}.

2.3. CEM deployment and analysis

Based on the methods published by Huang *et al.*, (2013), we used polyethersulfone CEMs, 47 and/or 90mm, 0.45µm pore size, Sterlitech Corporation and Millipore brands), to sample RM. Ambient atmospheric air was pumped at 1 L min^{-1} (47mm filters) or 4 L min^{-1} (90mm filters) from the same ambient air flow used by the Tekran® system and provided via two of the six side ports on the Tekran® 1104 manifold. Teflon filter holders (Savillex®) and 10 cm long ¼'' Teflon tubing were used to sample RM on CEMs as close as possible to the undisturbed ambient air flow as possible. We assume that RM did not degrade during the 63 milliseconds it took from the manifold flow to the CEM. A ball flow meter (Fisher Scientific), membrane pump (KNF), and gas volume meter (JHC) sampling train was used to regulate and quantify the total volume sampled, and was calibrated before and after each sampling period using a Bios Defender calibration unit. Teflon filter holders and tubing were acid washed, rinsed with MilliQ water, and double zip-lock bagged in a class-100 laminar flow hood before field deployment. Following sampling, CEMs were refrigerated (4^{o}C) and kept in the dark until analysis. To collect a sufficient quantity of RM, CEMs were deployed over 14 days.

In the laboratory, RM was extracted from each CEM in 10ml 20 vol.% inverse aqua regia (2:1 HNO_3: HCl, both double-distilled) in closed Teflon beakers for 12 hours at 120^{o}C. Hg concentrations of the extracts were determined by cold vapor atomic fluorescence spectrometry (CV-AFS) using a Brooks Rand Model III

AFS detector. The CV-AFS calibration range was 0-100 pg, made using dilutions of the NIST 3133 certified reference material (CRM), and had a limit of detection (LOD, 3σ of blanks) of 5.0 pg Hg. The CRM NRC ORMS-4 (certified at 26.2 ng L^{-1}) was analysed multiple times during each CV-AFS session with good results and a long-term precision of 10% (1σ). All CEM data are shown in Table 1 and completed with ancillary parameters in the supporting information (SI-2).

2.4. CEM Hg blanks

Extraction blanks of untreated CEMs were determined using the protocol describe in section 2.3. We have not attempted to decontaminate CEMs in acidic solutions, in fear of compromising the polyethersulfone structure and functional groups. Reagent blanks were 12 ± 14 pg of Hg (1σ, *n*=5). Sterlitech 47 and 90 mm CEM blanks were on average 464 ± 85 pg of Hg (1σ, *n*=9), and 3179 pg ± 564 of Hg (1σ, *n*=6) which can be considered as very elevated. Millipore 47 and 90 mm CEM blanks were 60 ± 13 pg of Hg (1σ, *n*=12), and 157 pg ± 23 pg of Hg (1σ, *n*=19). These results indicate that untreated CEM blanks scale with membrane surface area and depend on the manufacturer. The associated limits of detection (LOD, 3σ of blank) are 255, 1700, 39 and 69 pg Hg respectively. Typical amounts of Hg collected during bi-weekly sampling periods range from 1.32 to 10.3 ng Hg (Sterlitech) and from 0.49 to 2.6 ng Hg (Millipore) and were above the methods LOD. Because of the lower blanks, we switched halfway this study from Sterlitech to the cleaner Millipore membranes. This permitted us to explore daily sampling of RM, using the Millipore 90mm filters with the 157 pg blank and 69pg LOD. Five daily samples were collected from 1/12/2014 to 6/12/2014 which ranged from 300 to 1200 pg Hg. In the discussion below the corresponding filter blanks were subtracted for all samples.

3. Results and discussion

CEMs have been applied to manual trace level GOM sampling since the 1990s [17]. CEMs have recently regained interest as KCL-denuder based automated GOM collection is sensitive to bias [16, 25, 26]. Huang et al. performed QA/QC testing on GOM collection efficiency by 47mm, 0.45µm CEMs using controlled GOM

dosing by permeation sources. They observed no breakthrough of GOM from CEMs under a flow of 1 L min-1, deployed for 8h (experiments), or up to 7 days (outdoors ambient air). They also did not observe GEM capture on CEMs at experimental GEM levels <13 ng m^{-3}. Controlled GOM dosing of high levels (150-3000 pg m^{-3}) of gaseous and $HgBr_2$, $HgCl_2$, and HgO revealed 1.6, 2.4 and 3.7 times higher collection efficiency on CEMs compared to automated KCl-coated denuders. In this study we deployed 47mm, 0.45µm CEMs at 1 L min^{-1}, similar to Huang et al., in order to avoid breakthrough issues. We scaled up the flow rate to 4 L min^{-1} when using the larger 90mm 0.45µm CEMs.

Table 1 and SI-2 summarize CEM deployment conditions, RM_{CEM} amounts (pg Hg) and RM_{CEM} concentrations (pg m^{-3}), corresponding mean GEM_{TK}, GOM_{TK}, PBM_{TK}, the three consecutive $flush_{TK}$ blanks, and $pyrolizer_{TK}$ blank measured with the Tekran® system, and corresponding meteorology, CO and O3 from the PAES database [34]. Figure 1d shows that RM_{CEM} collected on the CEMs is 1.26x higher (r^2=0.85) than RM_{TK} concentrations from the automated Tekran® system, calculated as the sum of KCl-coated denuder based GOM_{TK} and quartz filter based PBM_{TK} concentrations. This result is similar to field deployment of CEMs at three sites by Huang et al. who found 1.5 ± 0.4 (1σ, r^2=0.53) times higher RM on CEMs than automated denuders and RPFs. A substantial fraction of RM_{TK} thus appears to be lost from the automated GOM_{TK} and PBM_{TK} collection system.

A second line of evidence for RM_{TK} loss from the automated system comes from the bi-hourly $flush_{TK}$ cycle(s) that immediately follow GOM_{TK} and PBM_{TK} collection, and precede the GOM_{TK} and PBM_{TK} desorption and quantification sequence. Figure 1a, which summarizes three years of data, shows a significant correlation (slope=0.48, r^2=0.62) between the amount of Hg released during the three 5-min flush cycles ($flush_{TK1-3}$) and the amount subsequently detected as GOM_{TK} during the three 5-min denuder desorption cycles. A similar correlation is obtained for bi-weekly integrated GOM_{TK} and $flush_{TK}$ shown in Figure 1a (slope of 0.46, r^2=0.83). Table 2 illustrates the sequence of events in detail for a 1-hour Hg speciation analysis periods that was part of high GOM event#7. The data correspond to the maximum GOM concentration of 167 pg m^{-3} detected during a long-lived (12h) GOM event that was discussed in detail elsewhere [33]. GOM event #7 is a

158 typical summer time phenomenon where upper free tropospheric air descends onto the PDM. Table 2
159 illustrates how the three $flush_{TK}$ cycles, which follow a full hour of automated GEM_{TK} analysis (last two cycles
160 only shown) and parallel GOM_{TK} and PBM_{TK} sampling, produce elevated $flush_{TK}$ readings of 27, 21, 11 pg m^{-3}.
161 Hg monitoring networks that use Tekran® systems use standard operating procedures (SOPs) that
162 calculate GOM and PBM as the sum of their respective three desorption cycles minus three times the value
163 of the third flush cycle. The initial two flush cycles are aimed at purging residual ambient air from the
164 system's dead volume, so that the third flush cycle is thought to represent the instrumental blank during
165 denuder and RPF heating cycles. With a dead volume of approximately 1 L, and ambient GEM_{TK} levels of 1.5
166 ng m^{-3}, the amount of Hg detected during the first flush cycle should be on the order of 1.5 pg Hg, and shown
167 in the first $flush_{TK1}$ cycle as 5 pg m^{-3} (taking into account relevant scaling factors). The total amount of Hg
168 detected during the three flush cycles ($flush_{TK}$= 27+21+11=59 pg m^{-3}) is one order larger than such a dead
169 volume effect. In order to understand which of the Tekran® components (i.e. inlet+denuder, RPF or
170 pyrolizer) releases Hg during the flush cycles we examined potential correlations between $flush_{TK}$ and PBM_{TK}
171 (r^2=0.01), pyrolizer cycle Hg, RH, CO, O_3, air temperature etc. yet found none (Figure 1c). The observation
172 that $flush_{TK}$ does not correlate with PBM_{TK} is also illustrated in Table 2 for a 2nd Hg speciation period that
173 represents the maximum PBM_{TK} concentration detected during PBM event #12 discussed in detail by Fu et
174 al., (2016). PBM event#12 is a typical winter time phenomena where cold middle to upper free tropospheric
175 air with elevated PBM (here 94 pg m^{-3}) is regularly observed at PDM. The total amount of Hg detected during
176 the three flush cycles (Hg_{flush} = 3.2+1.9+0=5.1 pg m^{-3}) is now similar to dead volume and regular instrumental
177 blank levels. We therefore strongly suspect that the elevated $flush_{TK}$ levels are caused by Hg loss from the
178 KCl-coated denuder and/or heated inlet and not the RPF or pyrolizer components.
179 The observation that Hg loss from the denuder during the flush cycles ($flush_{TK}$) is proportional to the
180 amount of GOM_{TK} detected during subsequent denuder heating cycles leads to the question whether we can
181 correct existing atmospheric Hg speciation datasets by adding $flush_{TK}$ to GOM_{TK}. In order to evaluate this we
182 need to understand whether GOM is only lost during the three 5-min flush cycles, when Hg-free air provided
183 by the Tekran® instrument flushes the inlet glassware, denuder, RPF and transfer tubing, or whether it is lost

continuously during the entire 1 hour sampling period. In Figure 1e we compare the sum of GOM_{TK}+PBM_{TK}+$flush_{TK}$ to RM_{CEM} and observed an excellent correlation (slope is 1.01, r^2=0.90) that is indicative of mass balance within the combined analytical uncertainties. The mass balance suggests that most likely GOM is not lost continuously during sampling, but occurs specifically during the introduction of Hg-free air during the flush cycles. We will now explore the use of Tekran® system PBM_{TK} observations to approximate GOM_{CEM} collected onto the CEMs by difference: $GOM_{CEM} = RM_{CEM} – PBM_{TK}$. In doing so we can estimate a GOM loss factor from KCl-coated denuder by comparing GOM_{CEM} to GOM_{TK}. Figure 1f shows that GOM_{CEM} is consistently higher by a factor of 1.56 than GOM_{TK} throughout the dataset, and regardless of filter type, sampling flow rate, weather conditions, air mass origin or sampling duration (1 day vs 2 weeks). RAMIX project results showed that experimental $HgBr_2$ retention was 1.6 and 2.0 times higher on CEMs than on automated denuders and a RM difference method, which may suggest that GOM at the PDM is predominantly in the $HgBr_2$ form[16, 35].

Figure 1a also shows that there is substantial variability in the ratio of $flush_{TK}$ to GOM_{TK} for each 2-hour period. At times $flush_{TK}$ represents only 20% of GOM_{TK} and at other times up to 200%, i.e. more GOM is lost than detected. Most likely this variability relates to the retention efficiency of different GOM compounds under the influence of different ambient air components such as O_3 and RH that are known to affect GOM retention on denuders [25, 26]. Using our parallel bi-weekly CEM and Tekran® observations we have explored whether the $flush_{TK}/GOM_{TK}$, $flush_{TK}/GOM_{CEM}$ or GOM_{TK}/GOM_{CEM} ratios correlate with RH, CO, O_3, GEM etc., but without succes. Most likely the longer 14-day CEM sampling period averages out variable GOM_{TK} loss conditions and trends are lost. We have further attempted to document more variable GOM_{CEM}/GOM_{TK} denuder loss factors and correlate these with $flush_{TK}/GOM_{TK}$ ratios by sampling RM_{CEM} at a daily frequency (and higher flow rate of 13 L min^{-1}) during the short period from 1/12/2016 to 5/12/2016. However, similar RM_{TK} and GOM_{TK} loss factors of 1.3 and 1.8 were observed as compared to bi-weekly integrated loss factors. Longer campaigns deploying even higher time resolution for CEMs (12h or less) will be required to study variations in GOM_{TK} loss due to GOM forms or different control factors.

Finally, we need to consider whether the GOM_{TK} lost from the denuder impacts GEM_{TK} measurements. Monitoring network SOPs recommend the following blank subtraction for PBM_{TK} and GOM_{TK} quantification (Table 2): sum of PBM (or GOM) cycles 1 to 3 – 3x $flush_{TK3}$. We observed that the three consecutive flush cycles 1-3 are also inter-correlated, e.g. $flush_{TK3}$ =0.06 x $flush_{TK1-3}$ (r^2=0.63; see SI-2). This suggests that $flush_{TK3}$ does not represent the instrument blank but is controlled by GOM loss at PDM. Since $flush_{TK3}$ is heavily impacted by GOM_{TK} loss the SOPs regularly overestimate the true PBM_{TK} and GOM_{TK} blanks and thereby further bias PBM_{TK} and GOM_{TK} to lower values. For the PDM dataset (SI-2) we therefore do not further correct the integrated PBM_{TK} and GOM_{TK} cycles, i.e. we do not correct for blanks and propose the following equations for GOM_{TK}* and PBM_{TK}* quantification:

$$GOM_{TK}^* = \sum GOM_{TK1-3} + \sum flush_{TK1-3}$$

$$PBM_{TK}^* = \sum PBM_{TK1-3}$$

In SI-2 we make available both the uncorrected and bias corrected (indicated by *, i.e GOM_{TK}*, PBM_{TK}*, GEM_{TK}*, RM_{TK}*) PDM Hg speciation dataset for the period 2011-2014, including ancillary parameters.

4. Implications for atmospheric Hg science

Our observation at PDM that denuder-based GOM_{TK} is approximately 1.6-fold underestimated may have important ramifications for global Hg cycling models that adjust GEM oxidation rates and mechanisms to fit denuder-based GOM_{TK} observations. Here we discuss PDM observations in comparison to other high-elevation sites, aircraft campaigns, and model results. Manual denuder-based GOM and/or PBM collection and quantification have been used by two aircraft studies [18, 36]. Continuous in-flight RM detection is more regularly performed using the Dual-channel Oxidized Hg System (DOhGS) method [9, 10, 18-20]. The DOhGS is a difference method, analysing total Hg (TM, by a pyrolizer) and GEM simultaneously on two parallel Tekran® 2537 analyzers, with a RM (= TM – GEM) LOD of 0.05 to 0.28 ng m^{-3}, sufficient for free tropospheric or stratospheric observations. Lyman and Jaffe (2011) reported elevated RM from 80 to 600 pg m^{-3} during an NCAR C-130 flight in a stratosphere-influenced air mass intersected at 6-7km altitude over the USA. Upper tropospheric air masses during the same flight were documented to contain <49 (LOD) to 220 ng m^{-3} of RM.

Subsequent deployment of the DOhGS during 19 NOMADSS flights over the central and eastern USA[10] documented RM levels above the LOD of 212 ± 112 pg m^{-3}. The GEOS-Chem Hg model (version 9-02) with bromine (Br) chemistry was not able to reproduce the observed RM (simulated RM of 67 ± 44 pg m^{-3}), suggesting either an underestimation of Hg(0) + Br oxidation rates or Br concentration. The highest RM concentrations, 300–680 pg m^{-3}, were observed in dry (RH < 35 %) and clean air masses during two flights over Texas at 5–7 km altitude and off the North Carolina coast at 1–3 km [10]. At the PDM we observed from 2012-2014 a total of 360 2h periods where GOM_{TK}* levels were >95th percentile of all GOM_{TK}* data. These high GOM* events are characteristic of free tropospheric air masses from various altitudes and had mean GOM_{TK}* and RM_{TK}* of 198±57 and 229±58 pg m^{-3} which is very similar to the mean RM level of 212 pg m^{-3} observed during the 19 NOMADSS flights. From 2012-2014 the maximum RM_{TK}* at PDM detected was 470 pg m^{-3}, and 47 GOM_{TK}* events had RM >300 pg m^{-3} which is also within the range of highest RM during NOMADSS. A more in-depth analysis of NOMADSS RF-06 flight where TM, RM, GEM and BrO were simultaneously observed in the free troposphere over Texas resolved the model vs. observation RM mismatch [9]. BrO was quantified using airborne differential optical absorption spectroscopy (DOAS). GEOS-Chem correctly predicted the RM-rich air mass, yet underestimated the magnitude of the enhancement. Modeled BrO mixing ratios (0.40 pptv) were significantly lower than in situ BrO measurements (1.9 pptv), leading the authors to suggest that Br concentrations in GEOS-Chem are biased low, causing the underestimated RM levels [9]. However, substantial disagreement exists on BrO levels in the free troposphere where DOAS techniques yield 2-4 times higher BrO levels (0.3 to 3.4 pptv [9, 37]) than those predicted (GEOS-Chem) or observed by chemical ionization mass spectrometry (CIMS, with nearly all tropospheric BrO <1 pptv LOD [38]). More accurate observations of BrO are therefore just as essential as accurate RM measurements in our quest to understand atmospheric GEM oxidation pathways.

Weiss-Penzias et al. (2015) reviewed GEM and RM (calculated as GOM+PBM from Tekran® analyzers) observations from five high-elevation sites and compared them with the GEOS-Chem model (version 9-01-01). RM levels in a free tropospheric subset of the data (identified as dry air with <75th percentile of water vapour levels at each site) show an annual mean of 34 pg m^{-3}. The highest RM concentrations occurred

during summertime dry air conditions at DRI, MBO and SPL (mean 61 pg m^{-3}) sites, but not LABS (due to humidity and high wet deposition). Non-bias corrected PDM observations for dry air (same <75th percentile criterion) show similar annual and summertime mean RM_{TK} levels of 51 and 44 pg m^{-3} respectively, and maximum RM in spring (63 pg m^{-3}). Annual mean modelled dry air RM of 84 g m^{-3} (Table SI-1 in ref. X) at the reviewed high-elevation sites over-predicted the reviewed observations, with annual mean RM of 34 pg m^{-3}, by a factor of 2.5 [8]. Annual mean, bias corrected, RM_{TK}* in dry air at PDM is 58 pg m^{-3}, which is still lower than the modelled RM of 84 pg m^{-3}, but only within a factor 1.5. It should be noted that dry air RM_{TK}* depends on the quartile used for water vapour screening [8], i.e. RM_{TK}* is 58, 66 and 80 pg m^{-3} for the 75th, 50th and 25th percentile WV-screening cut-off, the latter being much more relevant for delimiting free tropospheric dry air at PDM. Therefore, based on our PDM observations, mountain-top RM observations by denuder methods, when corrected for GOM_{TK} loss, would yield RM_{TK}* levels that are closer to simulated RM by the GEOS-Chem model and regardless of Br oxidation or OH-O_3 oxidation schemes used.

In conclusion, we showed that automated KCl-coated denuder based detection of GOM at the Pic du Midi can be corrected for GOM loss by including Hg detected during the instrument's flush cycles. Future research should further examine $flush_{TK}$ cycle behaviour and intercompare denuder-based GOM and PBM measurements with CEM based RM at a variety of sites, including but not limited to urban-industrial areas, remote terrestrial, marine boundary layer or polar sites. New studies should also attempt to understand which of the Tekran® inlet glass ware or the KCl-coated denuder is the primary cause of Hg loss during the flush cycles, and if possible investigate technical solution to the problem. More accurate RM observations at mountain-tops should also stimulate continued testing of GEM oxidation schemes in atmospheric Hg models.

Acknowledgments

This work was supported by research grant ERC-2010-StG_20091028 from the European Research Council to JES. We warmly acknowledge technical support from the UMS 831 Pic du Midi observatory team.

Figure captions

Figure 1a-f. Two-hourly (a) and bi-weekly (b-f) integrated relationships between automated Tekran® GOM_{TK}, PBM_{TK}, RM_{TK}, $flush_{TK1-3}$ measurements and manual CEM observations of RM_{CEM} at the Pic du Midi (all units in pg m^{-3}). $RM_{TK} = GOM_{TK} + PBM_{TK}$ nd $GOM_{CEM} = RM_{CEM} – GOM_{TK}$ (see text for details). Linear regression lines in panels c, d, e, f are forced through the origin, which has little effect on the R^2 values.

Table 1. Summary of the 6-month CEM and Tekran® (TK) inter-comparison results at the Pic du Midi. St47 = Sterlitech 47mm, and Mi90 = Millipore 90 mm CEMs. PBM_{TK} and GOM_{TK} are not corrected for 3x $flush_{TK3}$ blank. GOM_{TK} loss corrected RM_{TK}* = PBM_{TK} + GOM_{TK} + $flush_{TK1-3}$.

Sample	Start	End	RH	O3	CO	GEM_{TK}	PBM_{TK}	GOM_{T}	$Flush_{TK1}$	$Flush_{TK2}$	$Flush_{TK3}$	$Flush_{TK1-3}$	RM_{TK}*	RM_{CEM}
			%	ppbv	ppbv	ng m^{-3}	pg m^{-3}	pg m^{-3}	pg m^{-3}	pg m^{-3}	pg m^{-3}	pg m^{-3}	pg m^{-3}	pg m^{-3}
1-St47	18/6/14	4/7/14	84	52	80	1.40	20.8	14.7	4.3	1.2	0.3	5.8	41	43
2-St47	17/7/14	4/8/14	76	51	84	1.45	28.6	25.1	8.9	2.1	0.5	11.6	65	72
3-St47	4/8/14	26/8/14	76	47	94	1.50	41.5	22.0	6.2	1.6	0.3	8.1	100	120
4-St90	14/7/14	17/7/14	54	48	76	1.54	28.6	48.5	19.1	3.2	0.8	23.2	100	86
5-St90	14/7/14	17/7/14	54	48	76	1.54	28.6	48.5	19.1	3.2	0.8	23.2	72	71
6-St47	29/9/14	16/10/1	88	40	75	1.59	33.6	12.6	4.2	0.7	0.1	5.0	51	57
7-St90	29/9/14	16/10/1	88	40	75	1.59	33.6	12.6	4.2	0.7	0.1	5.0	51	47
8-St47	16/10/1	6/11/14	66	38	68	1.53	10.9	28.7	17.2	1.6	0.3	19.1	59	57
9-Mi90	6/11/14	20/11/1	84	42	89	1.43	13.1	7.0	7.2	1.4	0.4	9.0	29	39
10-Mi47	6/11/14	20/11/1	84	42	89	1.43	13.1	7.0	7.3	1.4	0.4	9.0	29	34
11-Mi90	1/12/14	2/12/14	95	39	104	1.62	15.3	20.9	5.5	0.7	0.3	6.5	43	50
12-Mi90	2/12/14	3/12/14	95	43	78	1.43	23.9	31.5	12.9	2.1	0.5	15.5	71	75
13-Mi90	3/12/14	4/12/14	95	44	79	1.40	20.6	41.1	21.5	1.8	1.0	24.4	86	84
14-Mi90	4/12/14	5/12/14	95	35	126	1.75	9.8	3.1	1.0	0.0	0.0	1.0	14	19
15-Mi90	5/12/14	6/12/14	94	32	138	1.68	8.9	2.0	1.2	0.0	0.0	1.2	12	11
16-Mi90	6/12/14	22/12/1	74	43	92	1.38	35.6	10.3	4.7	1.2	1.1	7.1	53	41
17-Mi47	5/12/14	22/12/1	75	42	94	1.39	34.7	10.0	4.6	1.2	1.1	6.9	52	53
18-Mi47	5/12/14	22/12/1	75	42	94	1.39	34.7	10.0	4.6	1.2	1.1	6.9	52	43

298 Table 2. Illustration of Hg loss during the flush cycles (in bold) of the automated Tekran® 1130/1135/2537B
299 system for two typical high GOM and high PBM events at the PDM discussed by Fu et al., 2016. For both
300 events the last two GEM_{TK} analyses of the 1h sampling period are shown. The Tekran® system subsequently
301 enters its 1h desorption period consisting of 3 flush cycles, pyrolizer heating cycle, 3 RPF heating cycles to
302 quantify PBM_{TK}, 3 denuder heating cycles to quantify GOM_{TK}, and two additional flush cycles. Flush blanks
303 correlate with GOM_{TK} levels, but not with PBM_{TK} suggesting continuous GOM loss from KCl-coated denuders
304 and/or inlet system.

305

High GOM event #7 - 16/05/2012

Local Time	Cycle Type	Peak Area	GEM ng m^{-3}	GOM/PBM /flush pg m^{-3}
05:25	GEM	26867	1.47	
05:30	GEM	26467	1.52	
05:35	flush 1	52592		**26.8**
05:40	flush 2	38508		**20.7**
05:45	flush 3	21263		**10.8**
05:50	Pyrolizer	16294		8.8
05:55	PBM 1	194972		99.3
06:00	PBM 2	11660		6.3
06:05	PBM 3	4770		2.4
06:10	GOM 1	302458		162.5
06:15	GOM 2	7553		3.8
06:20	GOM 3	3651		2.0
06:25	flush 4	0		0
06:30	flush 5	0		0

High PBM event #12 - 21/02/2012

Local Time	Flag	Peak Area	GEM ng m^{-3}	GOM/PBM /flush pg m^{-3}
07:20	GEM	28321	1.69	
07:25	GEM	26960	1.68	
07:30	flush 1	5704		**3.2**
07:35	flush 2	3240		**1.9**
07:40	flush 3	0		**0**
07:45	Pyrolizer	12242		7.1
07:50	PBM 1	143855		80.3
07:55	PBM 2	18719		10.9
08:00	PBM 3	4062		2.3
08:05	GOM 1	45615		26.5
08:10	GOM 2	1385		0.8
08:15	GOM 3	0		0
08:20	flush 4	0		0
08:25	flush 5	0		0

306

307

308

309 Figure 1a-f. Two-hourly (a) and bi-weekly (b-f) integrated relationships between automated Tekran® GOM_{TK},
310 PBM_{TK}, RM_{TK}, and $flush_{TK1-3}$ measurements and manual CEM observations of RM_{CEM} at the Pic du Midi (all
311 units in pg m^{-3}). $RM_{TK} = GOM_{TK} + PBM_{TK}$ and $GOM_{CEM} = RM_{CEM} – GOM_{TK}$ (see text for details). Linear regression
312 lines in panels c, d, e, f are forced through the origin, which has little effect on the R^2 values.

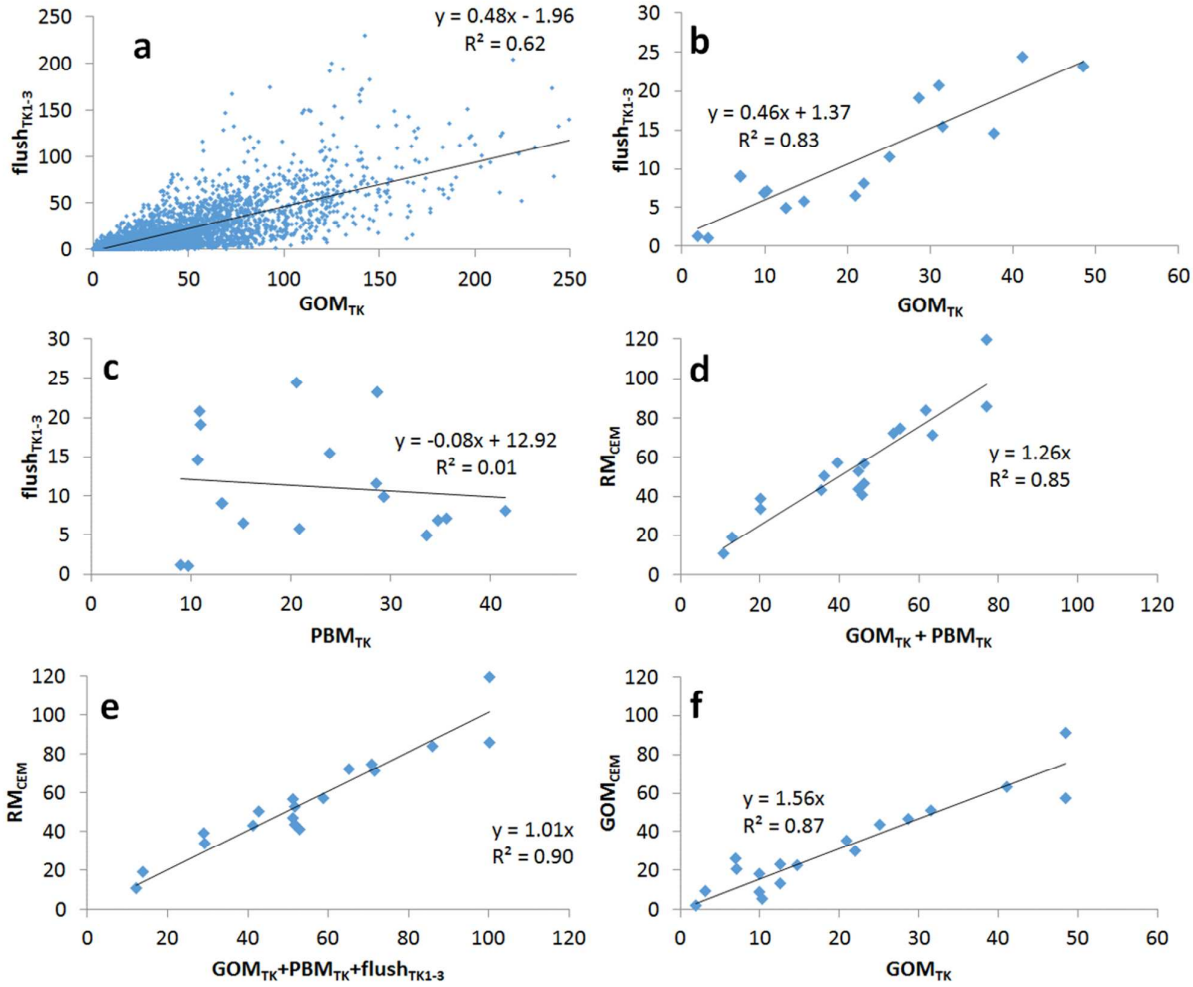

313

314

References

1. Amos, H. M.; Sonke, J. E.; Obrist, D.; Robins, N.; Hagan, N.; Horowitz, H. M.; Mason, R. P.; Witt, M.; Hedgecock, I. M.; Corbitt, E. S.; Sunderland, E. M., Observational and Modeling Constraints on Global Anthropogenic Enrichment of Mercury. *Environmental Science & Technology* **2015,** *49*, (7), 4036-4047.
2. UNEP, Global Mercury Assessment 2013: Sources, Emissions, Releases and Environmental Transport. UNEP Chemicals Branch, Geneva, Switzerland. **2013**.
3. Enrico, M.; Le Roux, G.; Marusczak, N.; Heimbürger, L.-E.; Claustres, A.; Fu, X.; Sun, R.; Sonke, J. E., Atmospheric mercury transfer to peat bogs dominated by gaseous elemental mercury dry deposition. *Environmental Science & Technology* **2016**.
4. Parrella, J. P.; Jacob, D. J.; Liang, Q.; Zhang, Y.; Mickley, L. J.; Miller, B.; Evans, M. J.; Yang, X.; Pyle, J. A.; Theys, N.; Van Roozendael, M., Tropospheric bromine chemistry: implications for present and pre-industrial ozone and mercury. *Atmospheric Chemistry and Physics* **2012,** *12*, (15), 6723-6740.
5. Amos, H. M.; Jacob, D. J.; Holmes, C. D.; Fisher, J. A.; Wang, Q.; Yantosca, R. M.; Corbitt, E. S.; Galarneau, E.; Rutter, A. P.; Gustin, M. S.; Steffen, A.; Schauer, J. J.; Graydon, J. A.; St Louis, V. L.; Talbot, R. W.; Edgerton, E. S.; Zhang, Y.; Sunderland, E. M., Gas-particle partitioning of atmospheric Hg(II) and its effect on global mercury deposition. *Atmospheric Chemistry and Physics* **2012,** *12*, (1), 591-603.
6. Seigneur, C.; Vijayaraghavan, K.; Lohman, K., Atmospheric mercury chemistry: Sensitivity of global model simulations to chemical reactions. *Journal of Geophysical Research - Atmosphere* **2006,** *111*, D22306.
7. Holmes, C. D.; Jacob, D. J.; Corbitt, E. S.; Mao, J.; Yang, X.; Talbot, R.; Slemr, F., Global atmospheric model for mercury including oxidation by bromine atoms. *Atmospheric Chemistry and Physics* **2010,** *10*, 12037–12057.
8. Weiss-Penzias, P.; Amos, H. M.; Selin, N. E.; Gustin, M. S.; Jaffe, D. A.; Obrist, D.; Sheu, G. R.; Giang, A., Use of a global model to understand speciated atmospheric mercury observations at five high-elevation sites. *Atmospheric Chemistry and Physics* **2015,** *15*, (3), 1161-1173.
9. Gratz, L. E.; Ambrose, J. L.; Jaffe, D. A.; Shah, V.; Jaegle, L.; Stutz, J.; Festa, J.; Spolaor, M.; Tsai, C.; Selin, N. E.; Song, S.; Zhou, X.; Weinheimer, A. J.; Knapp, D. J.; Montzka, D. D.; Flocke, F. M.; Campos, T. L.; Apel, E.; Hornbrook, R.; Blake, N. J.; Hall, S.; Tyndall, G. S.; Reeves, M.; Stechman, D.; Stell, M., Oxidation of mercury by bromine in the subtropical Pacific free troposphere. *Geophysical Research Letters* **2015,** *42*, (23).
10. Shah, V.; Jaegle, L.; Gratz, L. E.; Ambrose, J. L.; Jaffe, D. A.; Selin, N. E.; Song, S.; Campos, T. L.; Flocke, F. M.; Reeves, M.; Stechman, D.; Stell, M.; Festa, J.; Stutz, J.; Weinheimer, A. J.; Knapp, D. J.; Montzka, D. D.; Tyndall, G. S.; Apel, E. C.; Hornbrook, R. S.; Hills, A. J.; Riemer, D. D.; Blake, N. J.; Cantrell, C. A.; Mauldin, R. L., Origin of oxidized mercury in the summertime free troposphere over the southeastern US. *Atmospheric Chemistry and Physics* **2016,** *16*, (3), 1511-1530.
11. Laudal, D.; Nott, B.; Brown, T.; Roberson, R., Mercury speciation methods for utility flue gas. *Fresenius Journal of Analytical Chemistry* **1997,** *358*, (3), 397-400.
12. Stratton, W. J.; Lindberg, S. E., Use of a refluxing mist chamber for measurement of gas-phase mercury(II) species in the atmosphere. *Water Air and Soil Pollution* **1995,** *80*, (1-4), 1269-1278.
13. Landis, M. S.; Stevens, R. K.; Schaedlich, F.; Prestbo, E., Development and Characterization of an Annular Denuder Methodology for the Measurement of Divalent Inorganic Reactive Gaseous Mercury in Ambient Air. *Environmental Science and Technology* **2002,** *36*, 3000-3009.
14. Xiao, Z.; Sommar, J.; Wei, S.; Lindqvist, O., Sampling and determination of gas phase divalent mercury in the air using a KCl coated denuder. *Fresenius Journal of Analytical Chemistry* **1997,** *358*, (3), 386-391.
15. Lyman, S. N.; Gustin, M. S.; Prestbo, E. M.; Marsik, F. J., Estimation of dry deposition of atmospheric mercury in Nevada by direct and indirect methods. *Environmental Science & Technology* **2007,** *41*, (6), 1970-1976.
16. Huang, J.; Miller, M. B.; Weiss-Penzias, P.; Gustin, M. S., Comparison of Gaseous Oxidized Hg Measured by KCl-Coated Denuders, and Nylon and Cation Exchange Membranes. *Environmental Science & Technology* **2013,** *47*, (13), 7307-7316.

17. Bloom, N. S.; Prestbo, E. M.; Von der Geest, E. In *Determination of atmospheric gaseous Hg(II) at the pg/m3 level by collection onto cation exchange membranes, followed by dual amalgamation/cold caport atomic fluorescence spectrometry*, 4th International Conference on Mercury as a Global Pollutant, Hamburg, 1996; Ebinghaus, R.; Petersen, G.; Tumpling, U., Eds. GKKS: Hamburg, 1996; p 190.
18. Swartzendruber, P. C.; Jaffe, D. A.; Finley, B., Development and First Results of an Aircraft-Based, High Time Resolution Technique for Gaseous Elemental and Reactive (Oxidized) Gaseous Mercury. *Environmental Science & Technology* **2009,** *43*, (19), 7484-7489.
19. Ambrose, J. L.; Gratz, L. E.; Jaffe, D. A.; Campos, T.; Flocke, F. M.; Knapp, D. J.; Stechman, D. M.; Stell, M.; Weinheimer, A. J.; Cantrell, C. A.; Mauldin, R. L., Mercury Emission Ratios from Coal-Fired Power Plants in the Southeastern United States during NOMADSS. *Environmental Science & Technology* **2015,** *49*, (17), 10389-10397.
20. Lyman, S. N.; Jaffe, D. A., Formation and fate of oxidized mercury in the upper troposphere and lower stratosphere. *Nature Geoscience* **2011,** *5*, (2), 114-117.
21. Deeds, D. A.; Ghoshdastidar, A.; Raofie, F.; Guerette, E. A.; Tessier, A.; Ariya, P. A., Development of a Particle-Trap Preconcentration-Soft Ionization Mass Spectrometric Technique for the Quantification of Mercury Halides in Air. *Analytical Chemistry* **2015,** *87*, (10), 5109-5116.
22. Lan, X.; Talbot, R.; Castro, M.; Perry, K.; Luke, W., Seasonal and diurnal variations of atmospheric mercury across the US determined from AMNet monitoring data. *Atmospheric Chemistry and Physics* **2012,** *12*, (21), 10569-10582.
23. Sprovieri, F.; Gratz, L. E.; Pirrone, N., Development of a Ground-Based Atmospheric Monitoring Network for the Global Mercury Observation System (GMOS). In *Proceedings of the 16th International Conference on Heavy Metals in the Environment*, Pirrone, N., Ed. 2013; Vol. 1.
24. Cole, A. S.; Steffen, A.; Eckley, C. S.; Narayan, J.; Pilote, M.; Tordon, R.; Graydon, J. A.; St Louis, V. L.; Xu, X. H.; Branfireun, B. A., A Survey of Mercury in Air and Precipitation across Canada: Patterns and Trends. *Atmosphere* **2014,** *5*, (3), 635-668.
25. Lyman, S. N.; Jaffe, D. A.; Gustin, M. S., Release of mercury halides from KCl denuders in the presence of ozone. *Atmospheric Chemistry and Physics* **2010,** *10*, (17), 8197-8204.
26. Gustin, M. S.; Huang, J.; Miller, M. B.; Peterson, C.; Jaffe, D. A.; Ambrose, J.; Finley, B. D.; Lyman, S. N.; Call, K.; Talbot, R.; Feddersen, D.; Mao, H.; Lindberg, S. E., Do We Understand What the Mercury Speciation Instruments Are Actually Measuring? Results of RAMIX. *Environmental Science and Technology* **2013,** *DOI: 10.1021/es3039104*.
27. McClure, C. D.; Jaffe, D. A.; Edgerton, E. S., Evaluation of the KCl Denuder Method for Gaseous Oxidized Mercury using HgBr2 at an In-Service AMNet Site. *Environmental Science & Technology* **2014,** *48*, (19), 11437-11444.
28. Huang, J. Y.; Gustin, M. S., Uncertainties of Gaseous Oxidized Mercury Measurements Using KCl-Coated Denuders, Cation-Exchange Membranes, and Nylon Membranes: Humidity Influences. *Environmental Science & Technology* **2015,** *49*, (10), 6102-6108.
29. Ambrose, J. L.; Lyman, S. N.; Huang, J.; Gustin, M. S.; Jaffe, D. A., Fast Time Resolution Oxidized Mercury Measurements during the Reno Atmospheric Mercury Intercomparison Experiment (RAMIX). *Environmental Science & Technology* **2013,** *47*, (13), 7285-7294.
30. Gustin, M. S.; Huang, J. Y.; Miller, M. B.; Peterson, C.; Jaffe, D. A.; Ambrose, J.; Finley, B. D.; Lyman, S. N.; Call, K.; Talbot, R.; Feddersen, D.; Mao, H. T.; Lindberg, S. E., Do We Understand What the Mercury Speciation Instruments Are Actually Measuring? Results of RAMIX. *Environmental Science & Technology* **2013,** *47*, (13), 7295-7306.
31. Jaffe, D. A.; Lyman, S.; Amos, H. M.; Gustin, M. S.; Huang, J.; Selin, N. E.; Levin, L.; ter Schure, A.; Mason, R. P.; Talbot, R.; Rutter, A.; Finley, B.; Jaegle, L.; Shah, V.; McClure, C.; Arnbrose, J.; Gratz, L.; Lindberg, S.; Weiss-Penzias, P.; Sheu, G.-R.; Feddersen, D.; Horvat, M.; Dastoor, A.; Hynes, A. J.; Mao, H.; Sonke, J. E.; Slemr, F.; Fisher, J. A.; Ebinghaus, R.; Zhang, Y.; Edwards, G., Progress on Understanding Atmospheric Mercury Hampered by Uncertain Measurements. *Environmental Science & Technology* **2014,** *48*, (13), 7204-7206.

32. Gheusi, F.; Ravetta, F.; Delbarre, H.; Tsamalis, C.; Chevalier-Rosso, A.; Leroy, C.; Augustin, P.; Delmas, R.; Ancellet, G.; Athier, G.; Bouchou, P.; Campistron, B.; Cousin, J. M.; Fourmentin, M.; Meyerfeld, Y., Pic 2005, a field campaign to investigate low-tropospheric ozone variability in the Pyrenees. *Atmospheric Research* **2011,** *101*, (3), 640-665.
33. Fu, X. W.; Marusczak, N.; Heimbürger, L. E.; Sauvage, B.; Gheusi, F.; Sonke, J. E., Atmospheric mercury speciation dynamics at the high-altitude Pic du Midi Observatory, southern France. *Atmospheric Chemistry and Physics* **2016,** *16*, 5623-5639.
34. PAES Atmospheric Pollution at the Synpotic Scale network. http://paes.aero.obs-mip.fr/ accessed in 2016.
35. Finley, B. D.; Jaffe, D. A.; Call, K.; Lyman, S.; Gustin, M. S.; Peterson, C.; Miller, M.; Lyman, T., Development, Testing, And Deployment of an Air Sampling Manifold for Spiking Elemental and Oxidized Mercury During the Reno Atmospheric Mercury Intercomparison Experiment (RAMIX). *Environmental Science & Technology* **2013,** *47*, (13), 7277-7284.
36. Brooks, S.; Ren, X. R.; Cohen, M.; Luke, W. T.; Kelley, P.; Artz, R.; Hynes, A.; Landing, W.; Martos, B., Airborne Vertical Profiling of Mercury Speciation near Tullahoma, TN, USA. *Atmosphere* **2014,** *5*, (3), 557-574.
37. Wang, S. Y.; Schmidt, J. A.; Baidar, S.; Coburn, S.; Dix, B.; Koenig, T. K.; Apel, E.; Bowdalo, D.; Campos, T. L.; Eloranta, E.; Evans, M. J.; DiGangi, J. P.; Zondlo, M. A.; Gao, R. S.; Haggerty, J. A.; Hall, S. R.; Hornbrook, R. S.; Jacob, D.; Morley, B.; Pierce, B.; Reeves, M.; Romashkin, P.; ter Schure, A.; Volkamer, R., Active and widespread halogen chemistry in the tropical and subtropical free troposphere. *Proceedings of the National Academy of Sciences of the United States of America* **2015,** *112*, (30), 9281-9286.
38. Chen, D.; Huey, D.; Tanner, D. J.; Salawitch, R. J.; Anderson, D. C.; Wales, P. A.; Pan, L. L.; Atlas, E. L.; Hornbrook, R. S.; Apel, E. C.; Blake, N. J.; Campos, T. L.; Donets, V.; Flocke, F. M.; Hall, S. R.; Hanisco, T. F.; Hills, A. J.; Honomichl, S. B.; Jensen, J. B.; Kaser, L.; Montzka, D. D.; Nicely, J. M.; Reeves, J. M.; Riemer, D. D.; Schauffler, S. M.; Ullmann, K.; Weinheimer, A. J.; Wolfe, G. M., Airborne measurements of BrO and the sum of HOBr and Br2 over the Tropical West Pacific from 1 to 15km during the CONvective TRansport of Active Species in the Tropics (CONTRAST) experiment. *Journal of Geophysical Research* **2016,** *121*, 12,560-12,578.

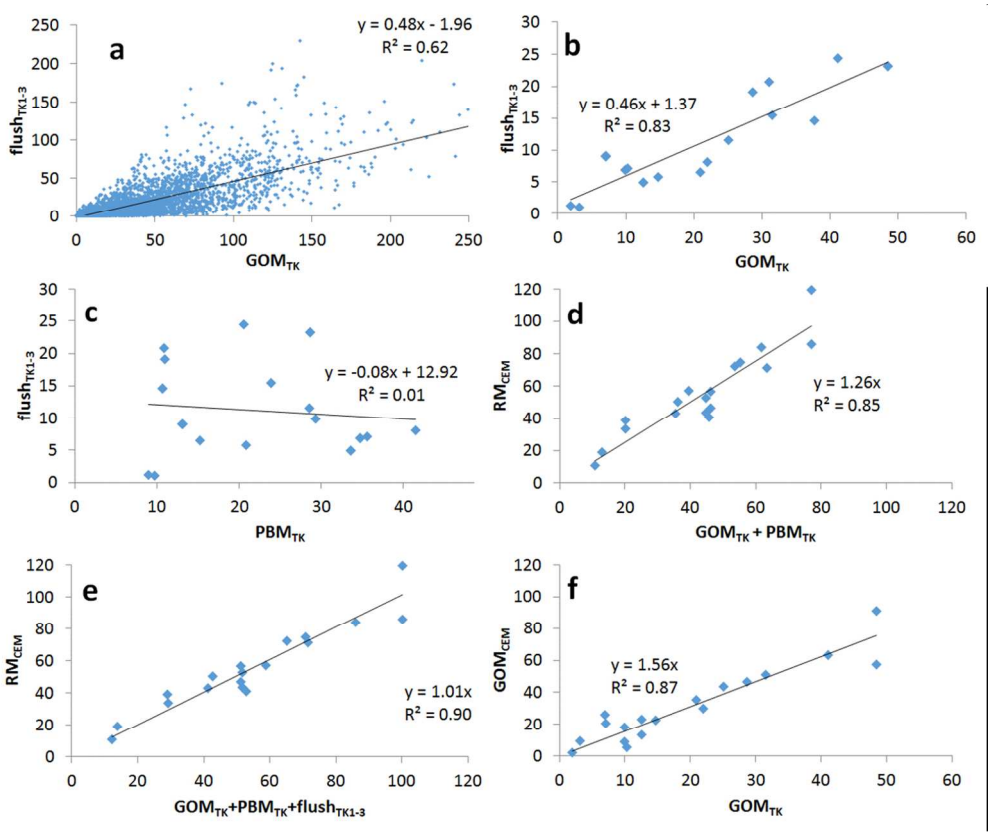

Figure 1a-f. Two-hourly (a) and bi-weekly (b-f) integrated relationships between automated Tekran® GOMTK, PBMTK, RMTK, and flushTK1-3 measurements and manual CEM observations of RMCEM at the Pic du Midi (all units in pg m-3). RMTK = GOMTK + PBMTK and GOMCEM = RMCEM – GOMTK (see text for details). Linear regression lines in panels c, d, e, f are forced through the origin, which has little effect on the R2 values.

220x182mm (150 x 150 DPI)

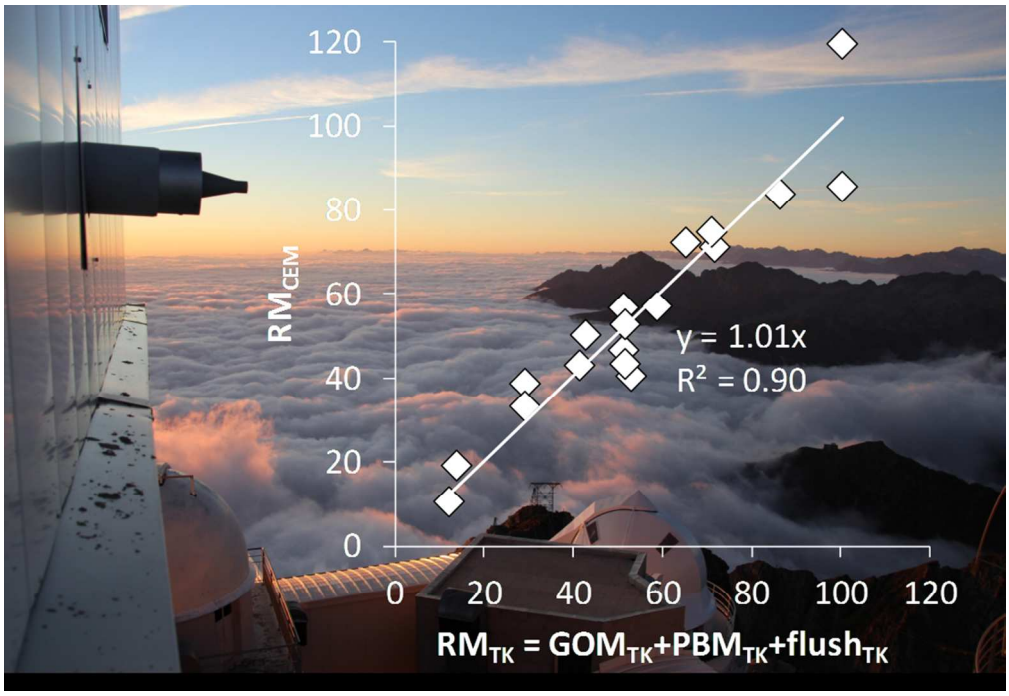

185x127mm (150 x 150 DPI)